INTERNATIONAL JOURNAL OF AUTOMOTIVE AND MECHANICAL ENGINEERING
ISSN: 2229-8649 e-ISSN: 2180-1606
VOL. 21, ISSUE 2, 2024, 11176 – 11190
DOI: https://doi.org/10.15282/ijame.21.2.2024.1.0864

RESEARCH ARTICLE

Modeling and Simulation of a Battery/Supercapacitor Hybrid Power Source for Electric Vehicles

C. L. Chen[1] and G. Z. Ren[2]

[1]School of Intelligent Manufacturing, Shandong Cultural Industry Vocational College, 266600, Qingdao, China
[2]School of Electromechanical and Automotive Engineering, Yantai University, 264005, Yantai, China

ABSTRACT - Environmental protection and energy conservation have become highly concerning themes. In the transportation field, green electric vehicles (EVs) are rapidly being promoted and applied, and power sources, as one of the core technologies, greatly affect the working performances of EVs. Currently, a single battery power supply is the mainstream configuration for EVs, but the instantaneous/short-term high-power output required by the battery for vehicle working conditions has a serious impact on the service life of the battery. As an effective solution, the battery/super-capacitor (SC) hybrid power source (HPS) has attracted increasing attention. This article proposes an improved semi-active battery/SC HPS, which can achieve multiple operating modes and fully utilize the advantages of the two power sources to effectively protect the battery. A fitness function is established with the optimization objective of minimizing the HPS cost and the number of cells in SC and battery as control variables. A genetic algorithm (GA) is adopted to optimize the HPS configuration based on the power required of the New European Driving Cycle (NEDC) working condition. The optimized number of battery cells is 777, much smaller than the 1191 calculated based on theoretical formulas. Additionally, a logic threshold strategy is introduced to flexibly control the collaborative work of the two power sources and achieve effective energy management. The availability of the presented control method of HPS in various working modes is verified through MATLAB/Simulink-based modeling and simulation. This work provides a theoretical reference for the application research of HPS in EVs.

ARTICLE HISTORY
Received : 11th May 2022
Revised : 07th June 2023
Accepted : 09th Mar. 2024
Published : 20th June 2024

KEYWORDS
Electric vehicle
Hybrid power source
Genetic algorithm

1.0 INTRODUCTION

A rapidly growing vehicle industry has brought about increasingly severe problems concerning energy crises and environmental pollution, making the development of efficient and clean new energy vehicles (NEVs) more urgent than ever [1-3]. Pure electric vehicle (PEV), as an ideal new energy vehicle, is clearly and increasingly being promoted and applied worldwide [4,5]. However, some concerns have been raised about PEV, such as short driving range, long charging time, poor power output, short battery life, and high replacement cost. Nowadays, multiple power sources and battery/super-capacitor (SC) hybrid power sources (HPS) as effective ways to solve the above problems have attracted more and more attention [6-8]. The battery/SC HPS can fully combine the stable energy output capability of the battery with the dynamic power output capability of SC, achieving complementary advantages between the two power sources. In battery/SC HPS, the battery as the primary energy source can output stable energy for the load, while the SC as the auxiliary power source can offer instantaneous high power or absorb braking energy, which fully reflects the respective advantages of the two power sources [9]. For instance, Ebkowski analyzed the working performance of the battery/SC HPS for electric vehicle (EV) [10]. The results show that HPS has apparent advantages over single-battery power sources. Kachhwaha et.al studied the output characteristics of battery/SC HPS for EVs [11]. The SC and battery are responsible for dynamic power and stable energy output respectively, thereby extending the battery life and driving range. Zhao et.al conducted a study of the application of a battery/SC HPS in a braking energy feedback system [12]. The results indicate that the regeneration efficiency can be effectively improved. Yang and Bai et.al studied the controller design methods of battery/SC HPS applied to EV [13,14]. Tshian et.al used the Python/MATLAB mixture model of SC to study the important role of SC in battery/SC HPS, which can effectively reduce battery stress and extend battery cycle life [15]. Ren et.al provided a detailed analysis of the application advantages, existing problems, key technologies, and application prospects of battery/SC HPS in NEVs [16].

As key technologies of HPS, configuration optimization, and energy management strategy optimization have greatly affected the performance of HPS, attracting the attention of researchers and resulting in some research results. For example, Fares et.al studied a variety of optimization algorithms, such as simulated annealing (SA) algorithm, genetic algorithm (GA), flower pollination algorithm (FPA), etc, to solve the HPS configuration optimization problem. And comparative analysis was conducted through simulation examples [17]. The conclusions can provide a reference for the size optimization study of HPS. Kamat et.al studied the size optimization of HPS for EVs based on the dynamic programming (DP) algorithm [18], which can minimize battery capacity loss while reducing the cost. Nuvvula et.al used

*CORRESPONDING AUTHOR | G. Z. Ren | ✉ renguizhou@tom.com

an improved particle swarm optimization (PSO) algorithm for configuration optimization of the power source [19], the results have proven that the scheme can cut system costs and battery degradation rate.

Si et.al studied the configuration optimization of HPS based on a combination of quantum computing and fuzzy control [20]. By establishing a low-cost and long-cycle life multi-objective optimization function, the optimal solution for HPS configuration was obtained. Zhang et.al used an improved non-dominated sorting genetic algorithm-II (NSGA-II) to achieve capacity configuration optimization for a multi-energy system, achieving good overall system performance [21]. This method provides a reference for optimizing the configuration of HPS in EVs. Li et.al adopted a combination of multiple optimization algorithms to achieve the power distribution and configuration optimization of a battery/SC HPS [22]. The results show that this method can fully utilize SC, effectively protect the battery, and improve energy efficiency.

Xu et.al used the reinforcement learning (RL) method to obtain the optimal energy efficiency of a battery/SC HPS and prolong battery life [23]. The results verify the effectiveness of the proposed method. Asensio et.al studied energy management of battery/SC HPS based on the model prediction method [24], which can effectively reduce battery stress and extend its service life, thereby increasing the range of EVs. Xu et.al used a Q-learning algorithm for the energy control strategy of a battery/SC HPS to improve energy efficiency and delay the rate of battery energy degradation, thus improving the driving range of EVs [25]. The results illustrate the validity of this method. So et.al studied the energy management strategy method of battery/SC HPS to fully utilize SC to protect the battery [26]. The results confirm that the battery life is prolonged by about 42% using this method. Also, energy management strategies of the battery/SC HPS were studied to rationally utilize the advantages of the two power sources and improve the performance of the vehicle [27-29]. Li and Lu et.al studied the power distribution strategies of battery/SC HPS based on optimization theory [30,31], with the main purpose of fully utilizing SC while the battery can output stable current, thereby effectively improving the battery life and vehicle endurance. Ren et.al comprehensively analyzed the performance of various optimization algorithms for power distribution of battery/SC HPS in EVs and conducted a comparative analysis of modeling and simulation based on different methods [32]. This study provides a reference for modeling methods and configuration optimization of battery/SC HPS.

Available researches are mainly based on conventional HPS structures (such as semi-active and fully active structures), while conventional HPS topologies have certain limitations in terms of the utilization rate of SC and the diversification of operating modes. In contrast, this article proposes a variable structure battery/SC HPS topology structure, which can realize two voltage outputs by controlling the switching between series and parallel connections of two sets of SCs, thereby achieving multiple working modes to fulfill the power demand of vehicle under complex driving conditions, and effectively improving the energy utilization rate of SCs. Firstly, considering the power requirement of a vehicle and the replacement cost of the HPS, the fitness function relationship between the cost of the HPS and the number of individual units of the two power sources is established, with the minimum cost of the HPS configuration as the optimization objective, and the number of SC and battery cells as control variables. And utilizing the strong global optimal searchability and ease of obtaining the optimal solution of GA to obtain the optimal goal, thereby reducing vehicle costs and improving economic efficiency. Then, an improved logic threshold control strategy is proposed to meet the multiple operating modes of the proposed HPS. This control strategy can effectively achieve the collaborative work of two power sources, improve the energy utilization of SC, and decrease the current change rate of the battery. Furthermore, to check the achievement of this work, a system model based on the Simulink environment is built, and simulation is implemented in conjunction with the New European Driving Cycle (NEDC) working condition.

2.0 THE PROPOSED HPS AND ITS OPERATING PRINCIPLE

A semi-active HPS topology for EV is proposed, as shown in Figure 1, which mainly consists of two SC banks (SC_1 and SC_2) capable of series and parallel switching, battery, and bi-directional power converter (BDPC1). T1, T2, and T3 control the switching of connection modes between the two SC banks.

T_1, T_2, and T_3 are commanded to be off, the two SC banks are switched to parallel connection for discharge. T_1 and T_3 are off, T_2 is on, and the two SC banks are switched to a series connection for discharge. T_1 and T_3 are switched on, T_2 is switched off, and the two SC banks are switched to parallel connections for charging. T_1, T_2, and T_3 are controlled to be disconnected, the two SC banks are switched to a series connection for charging.

K_1, K_2, and T_5 control the charging or discharge of battery. K_1 and K_2 are commanded to be disconnected, T_5 is connected, and the battery provides energy to the drive motor. K_1 is switched off, T_5 is switched on, K_2 is controlled by pulse width modulation (PWM) signal, the battery voltage is increased through BDPC1 and then provides energy to the drive motor. When the drive motor operates as a generator, if K_1 is on, K_2 and T_5 are off, BDPC1 is not required to perform power conversion, and energy is controlled to be fed back into the battery. K_2 and T_5 are switched off, K_1 is controlled by the PWM signal, the back electromotive force (EMF) of the drive motor is stepped down through BDPC1, and then the braking energy is controlled to be fed back into the battery. K_1, K_2, and T_5 are switched off, the battery is disconnected from the Bus terminal.

The switching of working modes of the two power sources is controlled by K_1, T_4, and T_5. T_4 is off, and T_5 is on, then the battery is discharged individually. If T_4 and T_5 are turned on, the battery and SC banks are discharged together. If K_1,

T_4, and T_5 are turned off. The SC banks recover energy separately. If T_4 and T_5 are off, K_1 is switched on or controlled by a PWM signal. The battery and SC banks recover energy together.

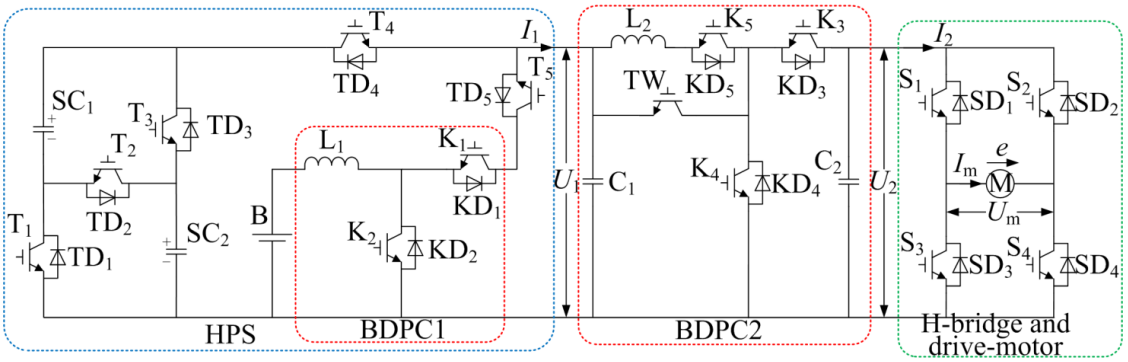

Figure 1. An EV propulsion system based on the proposed semi-active HPS

The working conditions of EVs mainly include starting, accelerating, cruising, and braking. According to the constantly changing working conditions of vehicles, the two power sources can be flexibly coordinated and matched to meet the power requirement. For example, when the vehicle starts, due to the small power required and the instantaneous large current demand, the SC can provide the required power separately to meet the instantaneous starting requirements and protect the battery. When the vehicle accelerates, the power can be provided separately by the SC, and as the demand for power increases, the required power can be jointly provided by two power sources. When the vehicle is cruising, stable energy can be provided by the battery, and when there is a dynamic change in demand power, it can be borne by the SC. When the vehicle brakes, the first choice is to feedback energy to the SC, or both power sources simultaneously.

The realizable working modes of the HPS mainly include power output mode and absorption power mode with boosting ability, power output mode, and absorption power mode with step-down capability. Assuming that the initial terminal voltages of SC_1 and SC_2 are the same (U_C), the initial voltage of the battery is U_B, and U_C=U_B, the terminal voltage of HPS is U_0. The supply voltage of the drive motor is U_m, and the back EMF of the drive motor is e.

(1) Output power mode I. When the drive motor is working in the motor state, if $U_m \leq U_C$, the battery is connected in parallel with the parallel-connected SC_1 and SC_2. The terminal voltage of HPS is U_C. The drive-motor current is adjusted by controlling the H-bridge inverter (as shown in Figure 1, it consists of power switches S_1 and SD_1, S_2 and SD_2, S_3 and SD_3, S_4 and SD_4).

(2) Output power mode II. If $U_m > U_C$, there are two working modes. When $U_C < U_m \leq 2U_C$, the battery is also connected in parallel with the parallel-connected SC_1 and SC_2. BDPC2 is in boost mode to step up the HPS voltage (U_C) to U_m. The other is, when $U_m > 2U_C$, SC_1, and SC_2 are switched to a series connection, BDPC1 is in boost mode to step up the battery voltage (U_B) to $2U_C$, BDPC2 is in boost mode to step up the HPS voltage ($2U_C$) to U_m.

(3) Absorb power mode I. When the drive motor is working in the generator state, if $e > U_C$, BDPC2 is in buck mode to step down the back EMF of the generator to the HPS voltage so that the energy generated by the generator is fed back to the HPS. If $e > 2U_C$, SC_1, and SC_2 are switched to the series connection. In this case, if K_1 is turned off, the battery is disconnected from the circuit, and the energy is only fed back to SC_1 and SC_2 connected in series. Otherwise, if K_1 is turned on, and BDPC1 is in buck mode, the energy can be fed back to the two power sources. If $U_C < e \leq 2U_C$, SC_1, and SC_2 are controlled in parallel, in this case, if K_1 is turned off, the battery is disconnected from the circuit, and the energy is only fed back to SC_1 and SC_2 connected in parallel, if K_1 is on, and BDPC1 is also in buck mode, and the energy can be controlled to flow to the two power sources.

(4) Absorb power mode II. If $e < U_C$, are switched to the parallel connection, BDPC2 is in buck mode to step up the back EMF to the terminal voltage of the HPS, so that energy generated by the generator is fed back to the HPS. It should be noted that in this case, due to the small back EMF, the drive motor produces only a small amount of energy that can be regenerated. Therefore, energy feedback control is generally not performed, but this working mode is feasible in principle.

For the multiple operating modes mentioned above of the HPS, the designed logic threshold control strategy is shown in Figure 2. P_{req} and P_{av} are the required and average required power of the vehicle under the NEDC working condition, respectively. P_{bat} and P_{bat_max} are the power and maximum power of the battery, respectively. Here, the battery power discharged at a current rate of 2C is taken as the ultimate power. P_{SC} is the power of SC banks, S_{SOC} is the state of charge (SOC) of SC banks, and S_{SOC_min} and S_{SOC_max} are the minimum and maximum of the SOC of SC banks, respectively. The process of power distribution of the HPS is shown in Figure 3.

3.0 OPTIMAL DESIGN OF HPS PARAMETERS BASED ON GENETIC ALGORITHM

The battery mainly provides stable energy output, and its number of cells determines the vehicle's driving range. As is well known, the instantaneous power of a battery is determined by its discharge rate. The higher the instantaneous

discharge rate, the greater the instantaneous power, but the battery life will also be shortened accordingly. The SC mainly provides the instantaneous high power required by the vehicle and feedbacks the braking energy. Therefore, when designing parameter matching for the HPS, the number of battery cells is calculated based on the driving range requirement, while the number of SC cells is calculated based on the peak power demand.

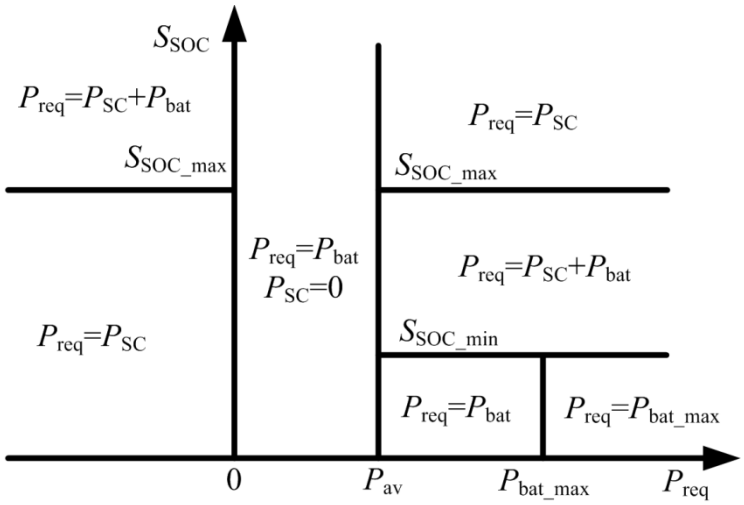

Figure 2. Schematic diagram of the logic threshold control strategy

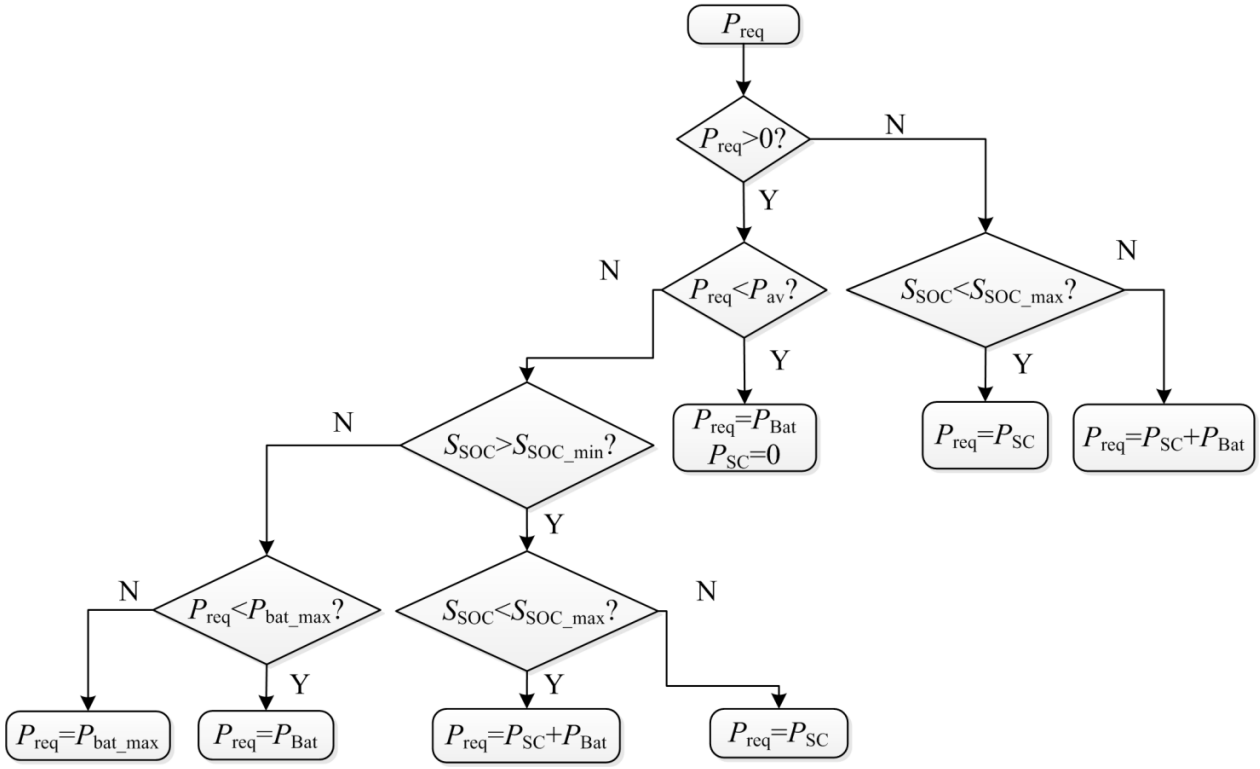

Figure 3. Power distribution flow chart

More importantly, the cost is an important consideration for the rationality of the HPS configuration, so the parameter-matching design of the HPS requires consideration of the cost. Designing a reasonable HPS configuration to minimize the cost of battery replacement is a vital issue that needs to be resolved.

The parameters of the selected lithium-iron-phosphate battery and SC here are shown in Table 1 and Table 2.

Table 1. The parameters of lithium-iron-phosphate battery cell

Name	Value
Rated capacity [Ah]	20
Rated voltage [V]	3.2
Internal resistance [mΩ]	10

Table 1. (cont.)

Name	Value
Charging cut-off voltage [V]	3.65
Discharge cut-off voltage [V]	2
Maximum charging rate [-]	1C
Maximum discharge rate [-]	3C
Operating temperature [℃]	-20-60
Weight [g]	530±5

Table 2. The parameters of SC cell

Name	Value
Rated capacity [F]	3000
Rated voltage [V]	2.7
Internal resistance [mΩ]	0.29
Maximum current [A]	1900
Power density [W/kg]	5.9
Energy density [Wh/kg]	6.0

According to the classic Arrhenius equation, the battery life can be expressed as:

$$Q_{\text{loss}}=Be^{\left[-\frac{E_a}{RT}\right]}(A_h)^z \tag{1}$$

$$A_h=NDC \tag{2}$$

where Q_{loss} is the capacity decay rate, B is the pre-exponential factor, z is the power coefficient, the value is 0.55, and E_a and R are the activation energy and molar gas constant, respectively. T and A_h are the Kelvin temperature and cumulative cyclic discharge, respectively. N is the number of the driving cycle, and D and C are the depth of discharge (DOD) and rated capacity of the battery, respectively. B and E_a are the battery parameters, whose values are affected by the discharge rate, which can be expressed as follows:

$$E_a=31700-370.3I_C \tag{3}$$

$$B=25990e^{-0.5572n}+10620e^{0.0071n} \tag{4}$$

where n represents the multiple of the discharge rate of the battery.

Then the values of pre-exponential factor B can be achieved, as shown in Table 3.

Table 3. The values of the pre-exponential factor

n	0.5C	1C	2C	6C
B	31630	27672	21681	12934

The battery life attenuation degree under a 1C discharge rate can be expressed as:

$$Q_1=B_1e^{\frac{-31700+370.3\times1}{RT}}(A_{h1})^{0.55} \tag{5}$$

The battery life attenuation degree under the nC discharge rate can be expressed as:

$$Q_n=B_ne^{\frac{-31700+370.3n}{RT}}(A_{hn})^{0.55} \tag{6}$$

Then, the model of the battery life attenuation degree can be obtained by formulas (5) and (6), which are expressed as follows:

$$Q_{n1}=B_1e^{\frac{-31329.7}{RT}}\left(\sqrt[0.55]{\left(1.169e^{-0.3375n}+0.146e^{0.1271n}\right)\cdot e^{(-0.1494+0.1494n)}}\cdot A_{hn}\right)^{0.55} \quad n\le 10 \tag{7}$$

Here, based on the NEDC working condition, GA is adopted to achieve the optimization of the HPS configuration parameters. The power demand is shown in Figure 4. It shows that the maximum demand power is 47.66kW.

GA stimulates the optimization process into a biological genetic process, encodes the initial population, and performs adaptive calculations on the encoded population. If the calculation result meets the condition, the algorithm directly performs the decoding operation and outputs the final result, then the calculation ends. If the calculation result does not

meet the need, the initial population is copied, crossed, and mutated to generate a new population, and the new population is again subjected to adaptive calculations until the result meets the conditions. According to the principle of survival of the fittest, in the process of repeatedly generating a new population, the new generation population obtained is closer to the optimal solution than the previous generation until the approximate optimal solution is obtained. GA has a solid global optimal searchability and cannot easily fall into a locally optimal solution. So, GA is used to optimize the cost of the HPS.

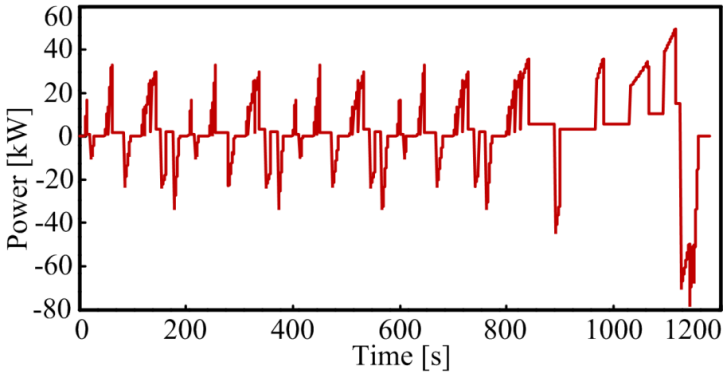

Figure 4. Power demand under the NEDC working condition

(1) Initialization of the population range. The number range of battery cells is determined by power requirement. The maximum driving range of the vehicle is selected as 300km. The vehicle is cruising at a constant speed of 60km/h, the DOD of the battery (η_B) does not exceed 80%, then the calculated demand power is P_{req}=6.766kW.

The vehicle driving range (S) can be expressed as:

$$S=\frac{E_B v}{P_{req}} \tag{8}$$

where E_B is the energy released by the battery, and v is the vehicle speed.

Then, E_B can be expressed as:

$$E_B=\frac{SP_{req}}{v}=C_{bat}U_{bat}N_{Bat}\eta_B \tag{9}$$

where C_{bat} is the capacity of the battery cell, U_{bat} is the voltage of the battery cell, and N_{Bat} is the number of battery cells. Since $\eta_B \leq 80\%$, then:

$$N_{Bat}\geq\frac{SP_{req}}{vC_{bat}U_{bat}\eta_B} \tag{10}$$

It is calculated that $N_{Bat}\geq 660.74$, then the number of battery cells is at least 661.

Taking the maximum required power under the NEDC working condition as the peak demand power of the battery, when the battery is individually discharged at a discharge rate of 1C, the maximum number of battery cells can be calculated as follows:

$$N_{Bat}\leq\frac{47.66\times 1000}{2\times 20}=1191.50 \tag{11}$$

Then, the maximum number of the battery cells is 1191.

(2) Determination of the fitness function. The fitness function is established according to the relationship between the vehicle cost and the number of cells of two power sources. The following three aspects need to be considered: satisfaction of power requirement, the relationship between the battery life and replacement cost, as well as the HPS cost.

The battery provides stable energy, and the SC is mainly responsible for peak current and recovery of braking power, so the available power of the HPS needs to meet:

$$P_{Bat}+P_{SC}\geq P_{Max} \tag{12}$$

where P_{Bat} and P_{SC} are the available power of battery and SC, respectively, P_{Max} is the maximum required power under the NEDC working condition, namely P_{Max}=47.66kW.

The cost of the HPS can be expressed as:

$$C_{HPS}=C_{Bat}+C_{SC}+C_{DC/DC} \tag{13}$$

where C_{HPS} is the cost of the HPS, and C_{Bat} and C_{SC} are the prices of battery and SC, respectively, and $C_{DC/DC}$ is the cost of the power converter.

Regarding the current market price, the price of the battery cell is 9.3 USD, the cost of the SC cell is 50.8 USD, and the cost of the power converter is 0.06 USD/W. The life cycle of the vehicle is selected as 220,000km, taking into account the HPS replacement cost during vehicle life. Since the cycle life of the SC and power converter is long enough, and replacement is not considered here, the replacement cost of the HPS can be regarded as the replacement cost of the battery. According to the classic Arrhenius theory, when the capacity of a battery decays to 20%, its output performance and safety performance will drop sharply. At this time, it can be considered that the battery should be replaced. The cost function of the HPS can be expressed as:

$$\begin{cases} C_{veh}=n_b C_b+n_u C_u+0.4\times 47660\times 2 & Q_n\leq 20 \\ C_{veh}=2n_b C_b+n_u C_u+0.4\times 47660\times 2 & Q_n>20 \end{cases} \tag{14}$$

where n_b and C_b are the number and price of the battery cell, respectively, and n_u and C_u are the number and price of the SC cell, respectively.

(3) Initial parameters setting. According to experience, the population number (*NP*) is generally 20 to 200, the crossover rate (*PC*) is 0.75 to 0.95, and the mutation rate (*Pm*) is 0.05 to 0.1. Then, the initial parameters are set as *NP*=20, *PC*=0.8, and *Pm*=0.1. In addition, the length of the genetic code string *L* takes 20.

The iterative process of the algorithm is shown in Figure 5. It can be seen that the optimal goal can be obtained within 100 iterations. The optimal value of the HPS cost is 14518USD, the number of battery cells is 777, the number of SC cells is 40, the cost of the battery is 6941USD, the cost of SC is 1899USD, and the cost of the power converter is 5677USD.

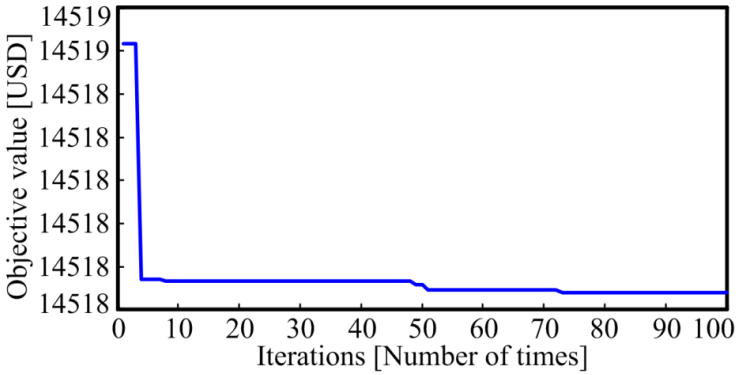

Figure 5. The iterative process of the algorithm

Here, the rated voltage of the battery pack and single SC bank (SC_1 or SC_2) is selected as 36V. Then, the battery pack consists of 11 cells connected in series into one circuit, and then 70 circuits in parallel. A single SC bank consists of 13 cells in series into one circuit, and then two circuits in parallel.

4.0 SIMULATION

To confirm the availability of the proposed scheme and the dynamic tracking characteristics of the control targets, the HPS configuration and control strategy models based on MATLAB/Simulink and Powerlib toolbox were established. The simulation model is shown in Figure 6, where the battery adopts the built-in model of Simulink, the SC selects the equivalent model of resistance and capacitance, and each power switch uses the Insulated Gate Bipolar Transistor (IGBT) in the Powerlib toolbox. The power converter model is composed of the IGBTs, inductance, and capacitance from the Powerlib toolbox. The H-bridge model is composed of four IGBTs from the Powerlib toolbox. The drive-motor model is an equivalent circuit model composed of resistance, inductance, and back EMF.

The control strategy model is shown in Figure 7, where the required power and SC SOC are used as logical threshold values. Based on the set values of the logical threshold signals, the working modes are controlled to switch. The model of the judgment module for the SC SOC is shown in Figure 8. According to the designed control strategy, based on the logic threshold signals, the controller needs to control the switching of the working modes of the HPS, the energy transmission, and the transformation of the power converter and H-bridge, thereby achieving the set control objectives. Here, an incremental proportion-integration-differentiation (PID) controller with good stability and practicality is used, and its model is shown in Figure 9. When the required voltage of the drive motor is less than 36V, neither BDPC1 nor BDPC2 performs a step-up conversion. The Bus voltage is given in Figure 10(a). The currents of the drive motor and HPS are shown in Figure 10(b) and (c), respectively. It can be seen that based on the step change of the drive-motor current, the actual drive-motor current can stably follow the set target, and the PID controller shows good dynamic responsiveness and stability. If the demand power is larger than the average demand power (here, its value is 2kW), the battery and SC are controlled to be connected in parallel to provide energy, where the SC provides a larger current output. Otherwise, if the demand power of the drive motor is less than the average demand power, the battery provides energy

separately. Correspondingly, when the vehicle is in a driving condition with low speed and high torque requirements such as starting, this working mode of HPS can greatly decrease the current output of the battery, effectively protect the battery, and thus prolong its service life.

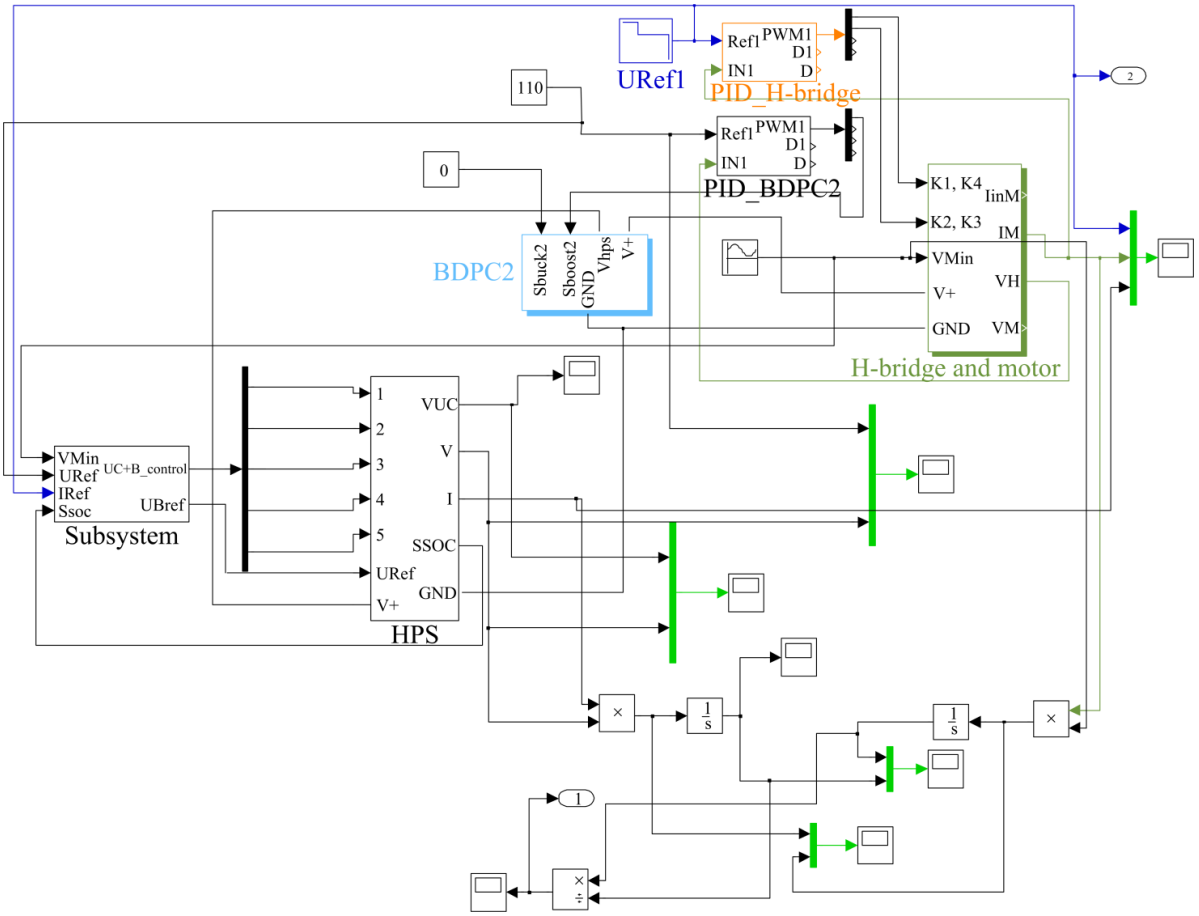

(a)

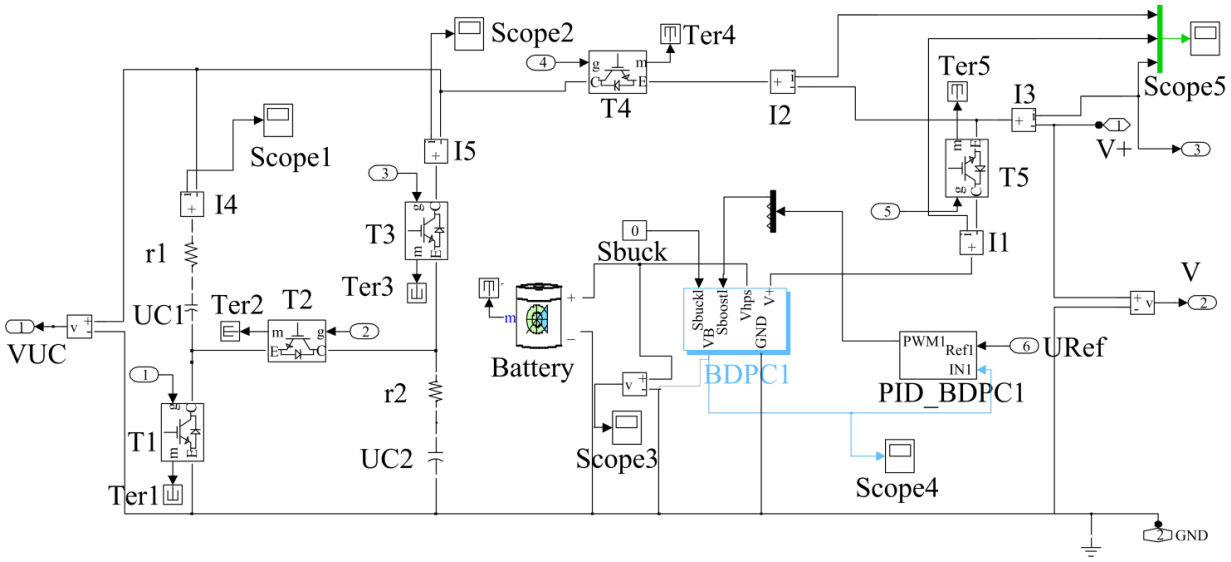

(b)

Figure 6. The simulation model (a) An overall model. (b) The HPS model

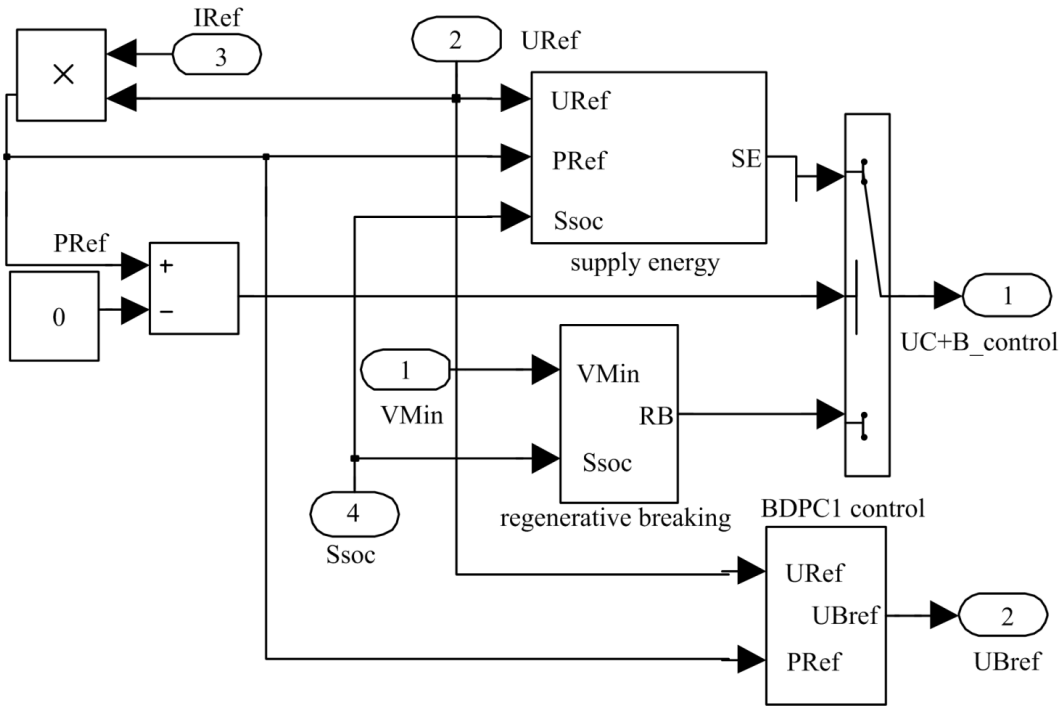

Figure 7. The control strategy model

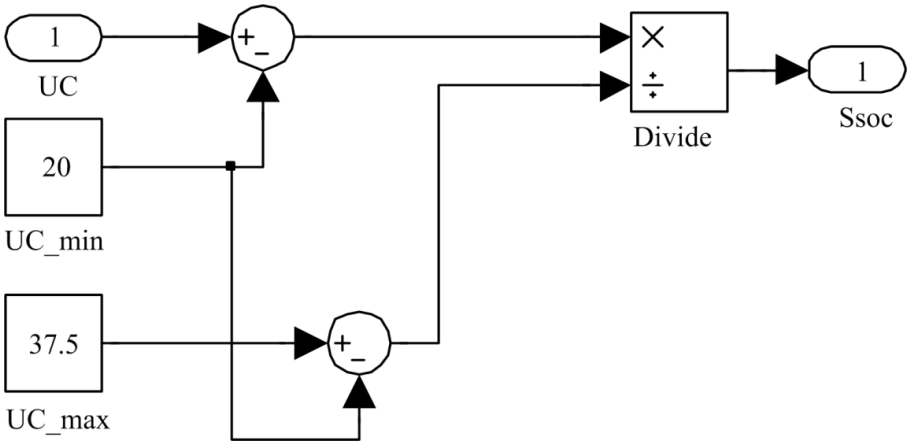

Figure 8. The judgment module of the SOC of SC

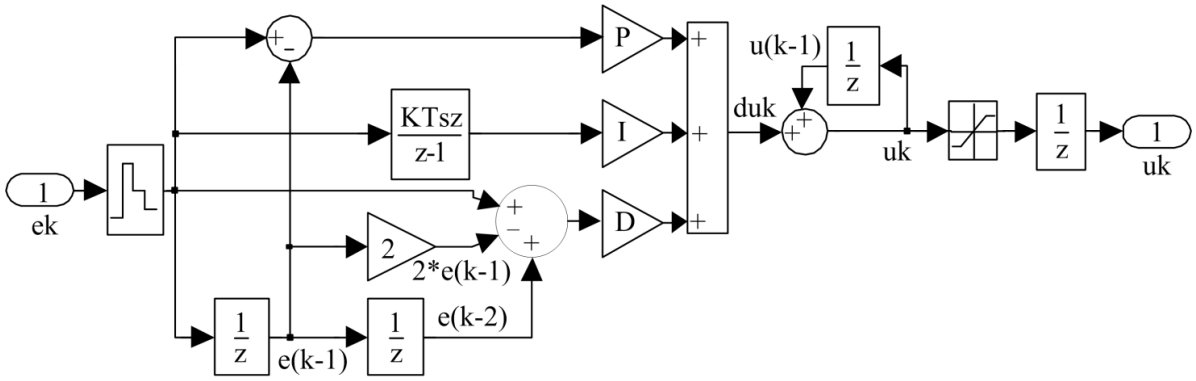

Figure 9. The incremental PID controller

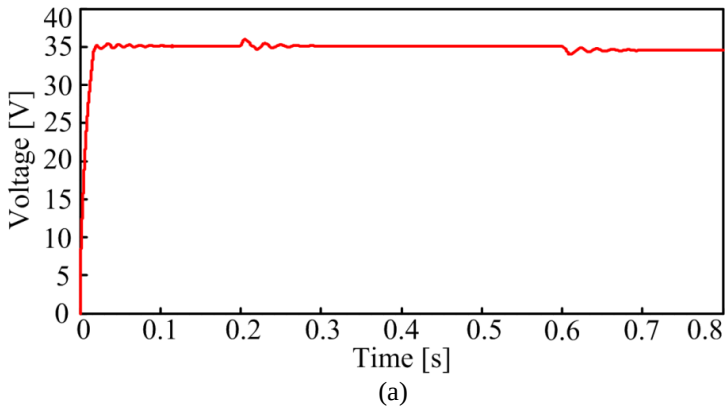

(a)

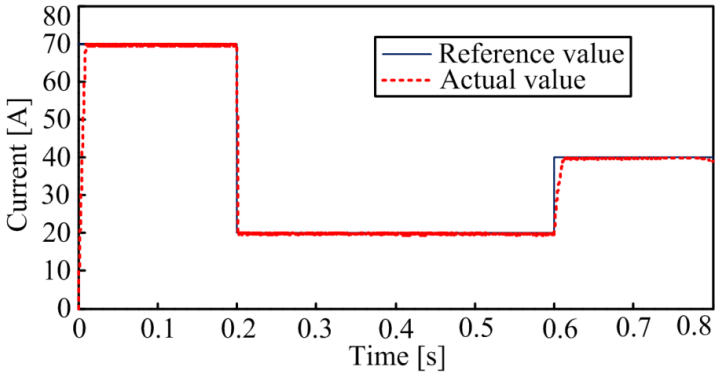

(b)

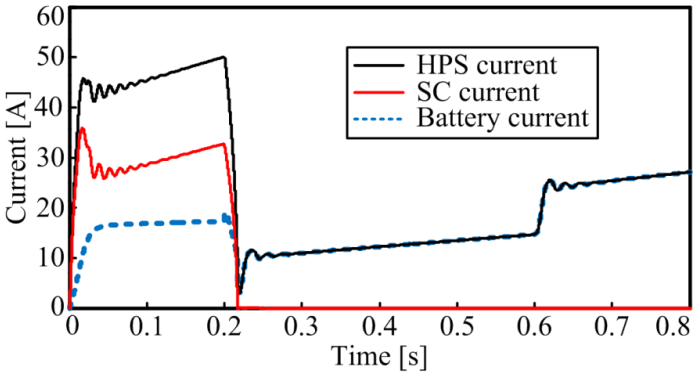

(c)

Figure 10. Some simulation results of providing energy in step-down mode, (a) Bus voltage, (b) Current of drive motor, (c) Currents of HPS, battery and SC

When the required voltage of the drive motor is greater than 36V and less than 72V, BDPC1 does not perform voltage conversion. BDPC2 works in boost mode. The reference of Bus voltage is set to 60V, the Bus voltage and terminal voltage of the HPS are shown in Figure 11(a). It can be seen that the Bus voltage quickly and almost without overshooting tracks the set target value. Only when the drive-motor current changes, there is a slight fluctuation in the Bus voltage, but it quickly stabilizes at the target value. The PID controller shows good stability. The currents of drive-motor and HPS are shown in Figure 11(b) and (c), respectively. It can be seen that when the drive-motor current undergoes step changes, the actual drive-motor current can also quickly track the target, and the PID controller shows good dynamic response and stability.

It shows that in the mode of co-supplying energy by the battery and SC banks, the battery outputs a stable current of about 15A, and the remaining demand current is supplemented by the SC banks to cut down the peak current output of the battery. Correspondingly, when the vehicle is in dynamically changing driving conditions, this working mode of the HPS makes the SC banks bear the dynamically changing power output, and the power output of the SC banks changes correspondingly with the dynamic change of power demand, which can ensure that the battery only provides a relatively stable energy output and effectively protect the battery.

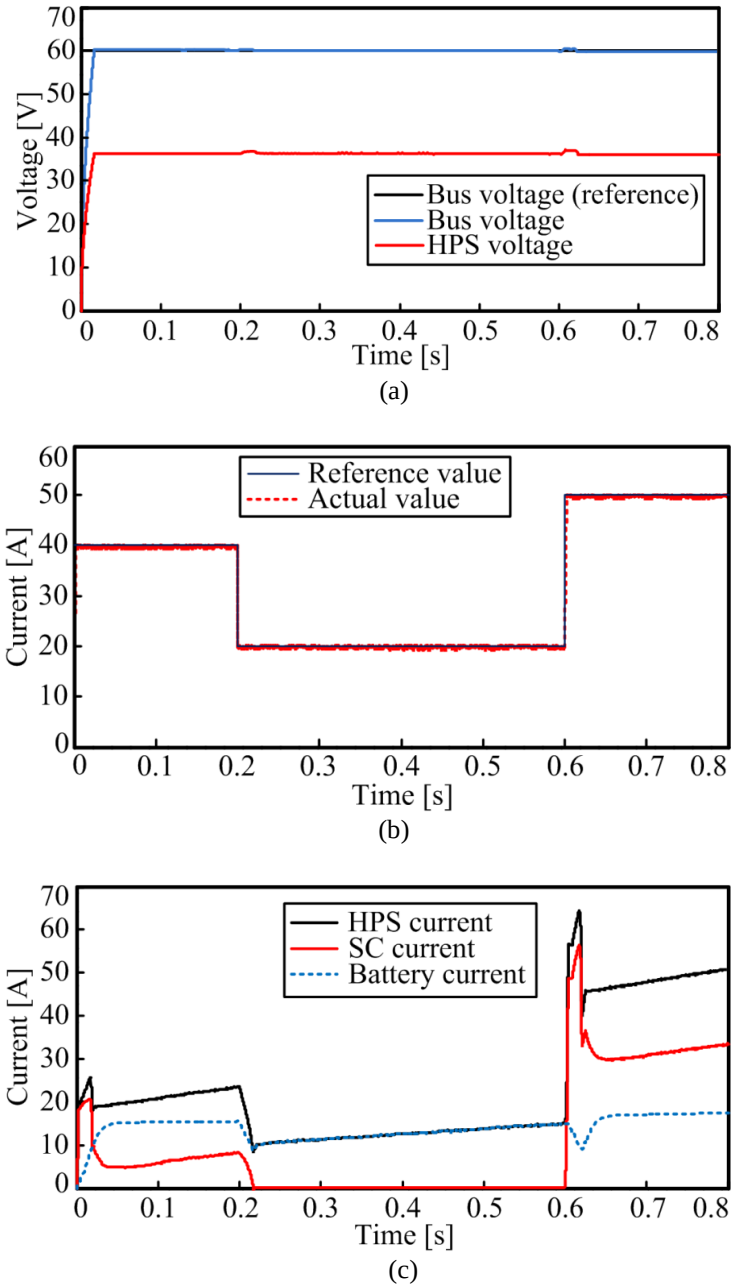

Figure 11. Some simulation results of providing energy in step-up mode, (a) Terminal voltage of the HPS and Bus voltage, (b) Current of drive-motor, (c) Currents of HPS, battery and SC

When the required voltage of the drive motor is greater than 72V, both BDPC1 and BDPC2 work in boost mode. Here, the reference of Bus voltage is set to 110V, the Bus voltage and HPS voltage are shown in Figure 12(a). It can be seen that the Bus voltage quickly and almost without overshooting tracks the set target value, and when the HPS voltage changes, the Bus voltage is also almost unaffected. The PID controller also shows good stability. The currents of drive-motor and HPS are shown in Figure 12(b) and (c), respectively. It can be seen that when the drive-motor current undergoes step changes, the actual value can also quickly track the reference value, and the PID controller shows good dynamic responsiveness and stability.

It also shows that in the mode of co-supplying energy by the battery and SC banks (in the interval of 0-0.6s), two SC banks are connected in series, and the HPS voltage is 72V. The battery outputs a small stable current of about 0.2A, while the SC banks bear the majority of the current output. Within an interval of 0.6s to 0.8s, the battery provides energy separately and the SC banks do not output current, the HPS voltage is 36V, which is boosted from BDPC2 to the target value of 110V for the bus voltage. Accordingly, when the vehicle is driving at a relatively high speed in a short time, this working mode of HPS can make the SC banks bear most of the power output, thus fully improving the energy utilization of SC banks. In the energy recovery, energy is only fed back to the SC banks, the initial voltage of a single SC bank is 24V. The drive motor works in a power generation state to convert vehicle kinetic energy into electrical energy, which is fed back into the SC banks. At the same time, it generates an electric braking force, which is related to the drive-motor current. The back EMF of the generator and HPS voltage are shown in Figure 13(a). It shows that the back EMF decreases

with the decrease of vehicle speed. When the back EMF e>72V, SC_1 and SC_2 are switched to a series connection to feedback energy (the initial terminal voltage at the beginning of the recovering energy mode is about 48V). When the back EMF e<72V, the two SC banks are switched to parallel connection to feedback energy (the terminal voltage is about 24V). The currents of the drive motor and HPS are shown in Figure 13(b). It can be seen that when the feedback current of the drive motor undergoes step changes, the actual value can also quickly track the reference value, and the PID controller shows good dynamic response and stability.

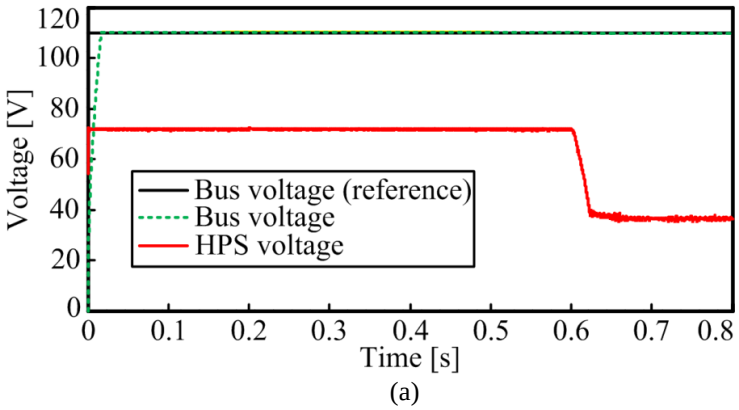

(a)

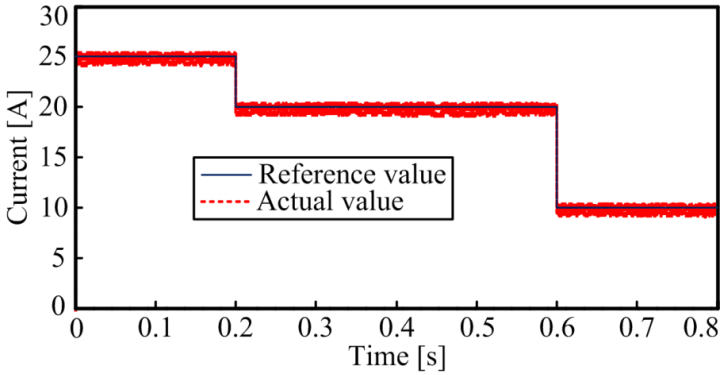

(b)

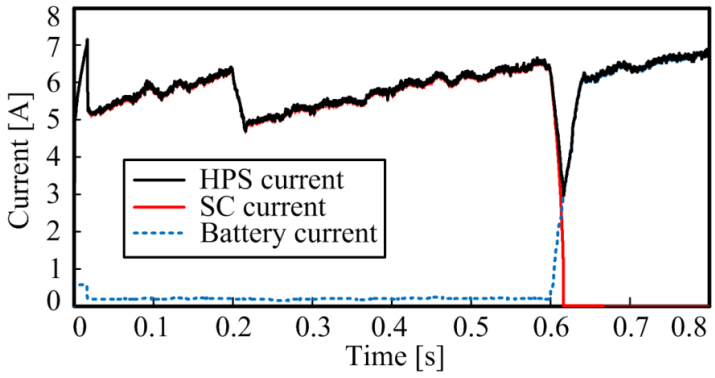

(c)

Figure 12. Some simulation results of providing energy in step-up mode II, (a) Terminal voltage of the HPS and Bus voltage, (b) Current of drive-motor, (c) Currents of HPS, battery and SC

5.0 CONCLUSION AND OUTLOOK

- A variable-voltage HPS topology that can realize real-time switching of SC banks in series and parallel is proposed. GA-based parameter optimization design method is adopted, in which main factors such as power demand, battery life, and cost are considered, the HPS cost is the optimization goal, thereby reasonably controlling the cost of the onboard power source. The optimized number of battery cells based on the NEDC working condition is 777, much smaller than the 1191 calculated based on theoretical formulas.

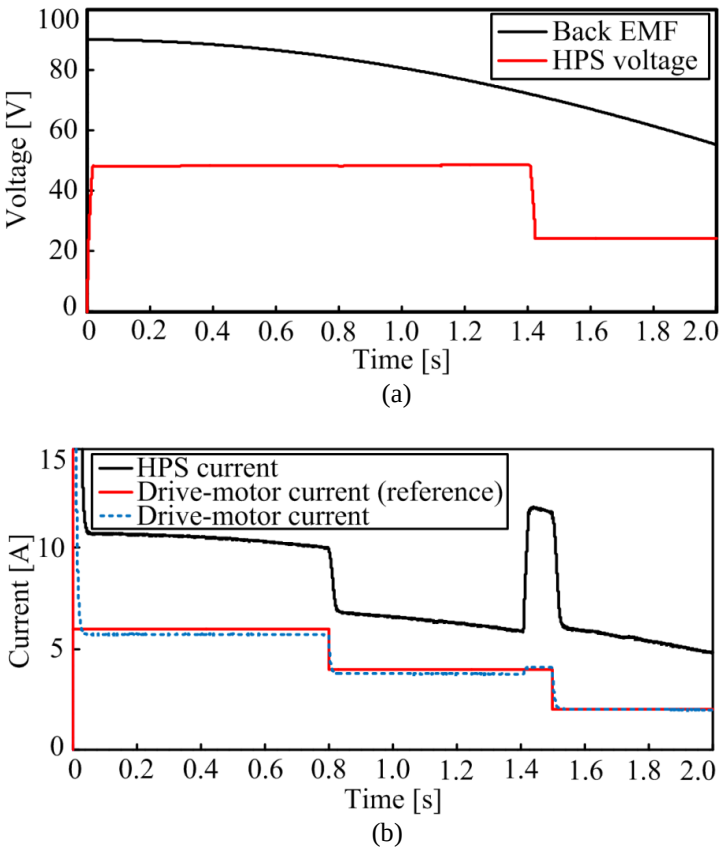

Figure 13. Some simulation results of recovering energy (a) Terminal voltage of the HPS and back EMF, (b) Currents of drive-motor and HPS

- Various working modes, as well as control of bus voltage, drive-motor current, and switching of SC banks, are all implemented in MATLAB-based simulation. The adopted power control strategy can fully leverage the advantages of SC in quickly adjusting dynamic power demands, increasing energy utilization, and reducing the peak current of the battery, which can prolong the battery life, and extend the vehicle's driving range. The designed logic threshold control strategy cannot achieve optimal control of power flow under complex driving conditions, thereby limiting the realization of optimal performance of the HPS. Therefore, in a follow-up study, intelligent algorithms will be introduced to optimize the power distribution and energy control of the HPS.
- Simulation results prove the validity and reliability of the designed scheme. Based on this work, future research will consider combining the proposed HPS with the vehicle model for simulation and optimization in environments closer to the actual working requirements of the vehicle and will pay relatively more attention to experimental evidence to further validate the efficiency and practicability of the proposed HPS and its control method.

6.0 ACKNOWLEDGEMENT

The work was supported by the Natural Science Foundation of Shandong Province [Grant No. ZR2020ME210]. We would like to thank the sponsor.

7.0 REFERENCES

[1] M. Waseem, A. F. Sherwani, and M. Suhaib, "Application of renewable solar energy with autonomous vehicles: a review," *Smart cities—Opportunities and Challenges Select Proceedings of ICSC 2019: Select Proceedings of ICSC 2019*, pp. 135-142, 2020.

[2] S. F. Qin, and Y. Q. Xiong, "Innovation strategies of Chinese new energy vehicle enterprises under the influence of non-financial policies: Effects, mechanisms and implications," *Energy Policy*, Vol. 164, p. 112946, 2022.

[3] Y. F. Chen, L. F. Ni, and K. L. Liu, "Innovation efficiency and technology heterogeneity within China's new energy vehicle industry: A two-stage NSBM approach embedded in a three-hierarchy meta-frontier framework," *Energy Policy.*, vol. 161, p. 112708, 2022.

[4] M. Waseem, A. F. Sherwani and M. Suhaib, "Highway gradient effects on hybrid electric vehicle performance," *Smart cities—Opportunities and Challenges Select Proceedings of ICSC 2019: Select Proceedings of ICSC 2019*, pp. 583-592, 2020.

[5] M. Waseem, A. F. Sherwani, and M. Suhaib, "Driving pattern-based optimization and design of electric propulsion system for three-wheeler battery vehicle," *International Journal of Performability Engineering*, vol. 16, no. 3, pp. 342-353, 2020.

[6] G. Z. Ren, G. Q. Ma, and N. Cong, "Review of electrical energy storage system for vehicular applications," *Renewable and Sustainable Energy Reviews*, vol. 41, pp. 225-236, 2015.

[7] M. Waseem, A. F. Sherwani, and M. Suhaib, "Integration of solar energy in electrical, hybrid, autonomous vehicles: a technological review," *SN Applied Sciences*, vol. 1, p. 1459, 2019.

[8] M. Waseem, M. Suhaib, and A. F. Sherwani, "Modelling and analysis of gradient efect on the dynamic performance of three-wheeled vehicle system using Simscape," *SN Applied Sciences*, vol. 1, p. 225, 2019.

[9] R. Xiong, H. Chen, C. Wang, and F. Sun, "Towards a smarter hybrid energy storage system based on battery and ultracapacitor-A critical review on topology and energy management," *Journal of Cleaner Production*, vol. 202, pp. 1228-1240, 2018.

[10] A. Ebkowski, "Studies of energy consumption by a city bus powered by a hybrid energy storage system in variable road conditions," *Energies*, vol. 12, No. 5, p. 951, 2019.

[11] A. Kachhwaha, G. I. Rashed, and A. R. Garg, O. P. Mahela, B. Khan, M. B. Shafik, *et al*., "Design and performance analysis of hybrid battery and ultracapacitor energy storage system for electrical vehicle active power management," *Sustainability-Basel*, vol. 14, no. 2, p. 776, 2022.

[12] W. Z. Zhao, G. Wu, C. H. Wang, L. Yu and Y. Li, "Energy transfer and utilization efficiency of regenerative braking with hybrid energy storage system," *Journal of Power Sources*, vol. 427, pp. 174-183, 2019.

[13] B. Yang, J. Wang, X. Zhang, J. Wang, H. Shu, S. Li, *et al*., "Applications of battery/supercapacitor hybrid energy storage systems for electric vehicles using perturbation observer based robust control," *Journal of Power Sources*, vol. 448, p. 227444, 2020.

[14] Z. Bai, Z. Yan, X. Wu, J. Xu and B. Cao, "H∞ control for battery/supercapacitor hybrid energy storage system used in electric vehicles," *International Journal of Automotive Technology*, vol. 20, no. 6, pp. 1287-1296, 2019.

[15] C. T. Tshian and P. Umenne, "The impact of the Electric Double-Layer Capacitor (EDLC) in reducing stress and improving battery lifespan in a Hybrid Energy Storage System (HESS) System," *Energies*, vol. 15, no. 22, p. 8680, 2022.

[16] G. Z. Ren, H. R. Wang, C. L. Chen, and J. Wang, "An energy conservation and environmental improvement solution-ultra-capacitor/battery hybrid power source for vehicular applications," *Sustainable Energy Technologies and Assessments*, vol. 44, p. 100998, 2021.

[17] D. Fares, M. Fathi, and S. Mekhilef, "Performance evaluation of metaheuristic techniques for optimal sizing of a stand-alone hybrid PV/wind/battery system," *Applied Energy*, 2022, p. 305, 2022.

[18] S. Kamat, K. Follen, and A. Chunodkar, "A two stage dynamic programming-based sizing of hybrid energy storage system for hybrid electric vehicles," *SAE International Journal of Electrified Vehicles*, vol. 11, no. 1, pp. 33-44, 2022.

[19] R. S. S. Nuvvula, K. S. Teegala, E. Devaraj, S. I. Taheri, M. Irfan and K. S. Teegala, "Multi-objective mutation-enabled adaptive local attractor quantum behaved particle swarm optimisation based optimal sizing of hybrid renewable energy system for smart cities in India," *Sustainable Energy Technologies and Assessments*, vol. 49, p. 101689, 2022.

[20] Y. P. Si, R. J. Wang, S. Q. Zhang, W. Zhou, A. Lin, and G. Zeng, "Configuration optimization and energy management of hybrid energy system for marine using quantum computing," *Energy*, vol. 253, p. 124131, 2022.

[21] Y. Zhang, H. X. Sun, J. X. Tan, Z. Li, W. Hou, and Y. Guo, "Capacity configuration optimization of multi-energy system integrating wind turbine/photovoltaic/hydrogen/battery," *Energy*, vol. 252, p. 124046, 2022.

[22] M. C. Li, L. Wang, Y. J. Wang and Z. Chen, "Sizing optimization and energy management strategy for hybrid energy storage system using multi-objective optimization and random forests," *IEEE Transactions on Power Electronics*, vol. 36, no. 10, pp. 11421-11430, 2021.

[23] B. Xu, Q. Zhou, J. Z. Shi, and S. Li, "Hierarchical Q-learning network for online simultaneous optimization of energy efficiency and battery life of the battery/ultracapacitor electric vehicle," *Journal of Energy Storage*, vol. 46, p. 103925, 2022.

[24] E. M. Asensio, G. A. Magallán, L. Pérez and C. H. D. Angelo, "Short-term power demand prediction for energy management of an electric vehicle based on batteries and ultracapacitors," *Energy*, vol. 247, p. 123430, 2022.

[25] B. Xu, J. Z. Shi, S. X. Li, H. Li and Z. Wang, "Energy consumption and battery aging minimization using a q-learning strategy for a battery/ultracapacitor electric vehicle," *Energy*, vol. 229, p. 120705, 2021.

[26] K. M. So, G. S. Hong, and W. F. Lu, "An improved speed-dependent battery/ultracapacitor hybrid energy storage system management strategy for electric vehicles," *Proceedings of the Institution of Mechanical Engineers, Part D: Journal of Automobile Engineering*, vol. 235, no. 14, pp. 3459-3473, 2021.

[27] T. C. Do, H. Truong, H. V. Dao, C. M. Ho, X. D. To, T. D. Dang *et al*., "Energy management strategy of a PEM fuel cell excavator with a supercapacitor/battery hybrid power source," *Energies*, vol. 12, no. 22, p. 4362, 2019.

[28] S. Mehdi, S. Abdeddaim, A. Betka, A. Djerdir, S. Drid, and M. Tiar, "Fuzzy-Super twisting control implementation of battery/super capacitor for electric vehicles," *ISA Transactions*, vol. 95, pp. 243-253, 2019.

[29] Q. Zhang, L. Wang, G. Li, and Y. Liu, "A real-time energy management control strategy for battery and supercapacitor hybrid energy storage systems of pure electric vehicles," *Journal of Energy Storage*, vol. 31, p. 101721, 2020.

[30] G. Li, Z. Yang, B. Li, and H. Bi, "Power allocation smoothing strategy for hybrid energy storage system based on Markov decision process," *Applied Energy*, vol. 241, pp. 152-163, 2019.

[31] X. Y. Lu, Y. J. Chen, and M. F. Fu and H. Wang, "Multi-objective optimization-based real-time control strategy for battery/ultracapacitor hybrid energy management systems," *IEEE Access*, vol. 7, pp. 11640-11650, 2019.

[32] G. Z. Ren, J. Z. Wang, Y. Y. Li, and G. Zhang, "Power distribution optimization of a fully active hybrid energy storage system configuration for vehicular applications," *Journal of Industrial Information Integration*, vol. 33, p. 100459, 2023.